

Foreword

In thermographic works, images are very important. It is not always possible to reproduce them with the desired quality, mainly for cost reasons, especially for colour images.

To solve this problem, the QIRT Journal Portfolio presents all the images given in the papers published in the Journal issues. Readers can load and print these images to help them to better appreciate the works presented in the journal.

Quantitative infrared thermography applied to blow moulding process: measurement of a heat transfer coefficient Local thermal diffusivity measurement
 by Serge Monteix, Yannick Le Maout, Fabrice Schmidt, Jean Paul Arcens
 QIRT Journal, 1, 2, pp.133-150

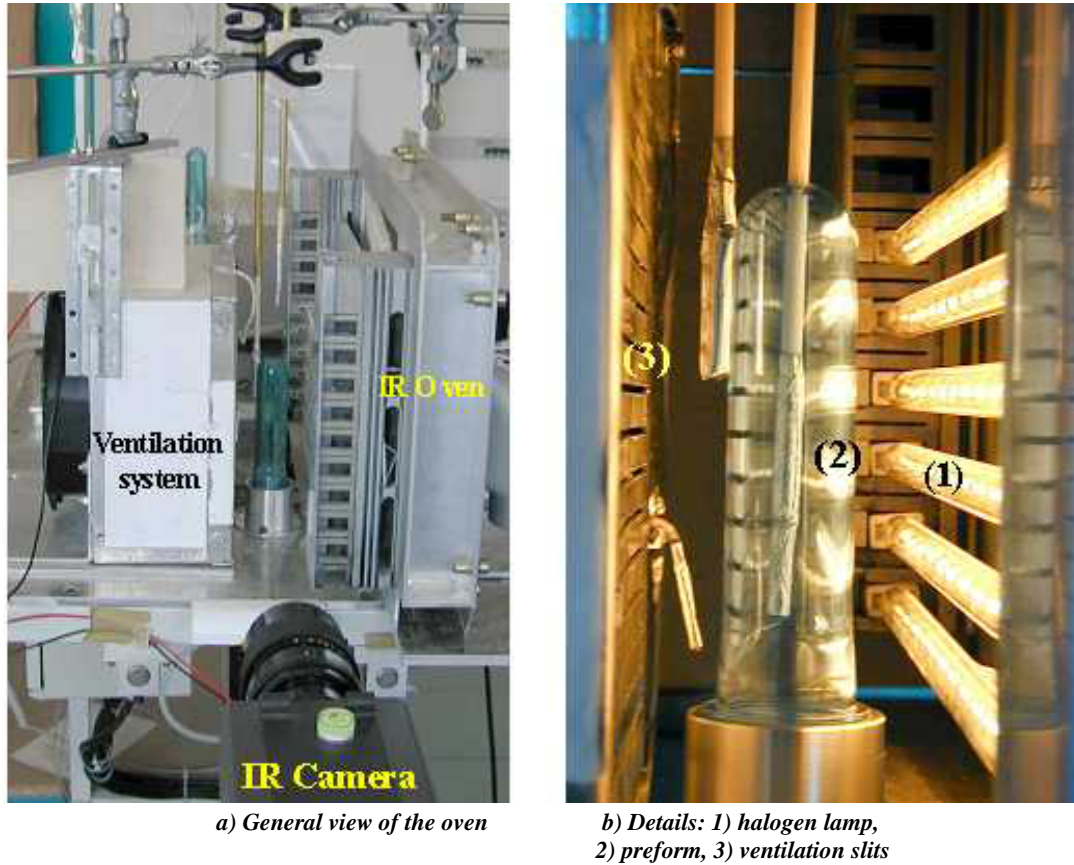


Figure 1. Experimental set-up and infrared oven

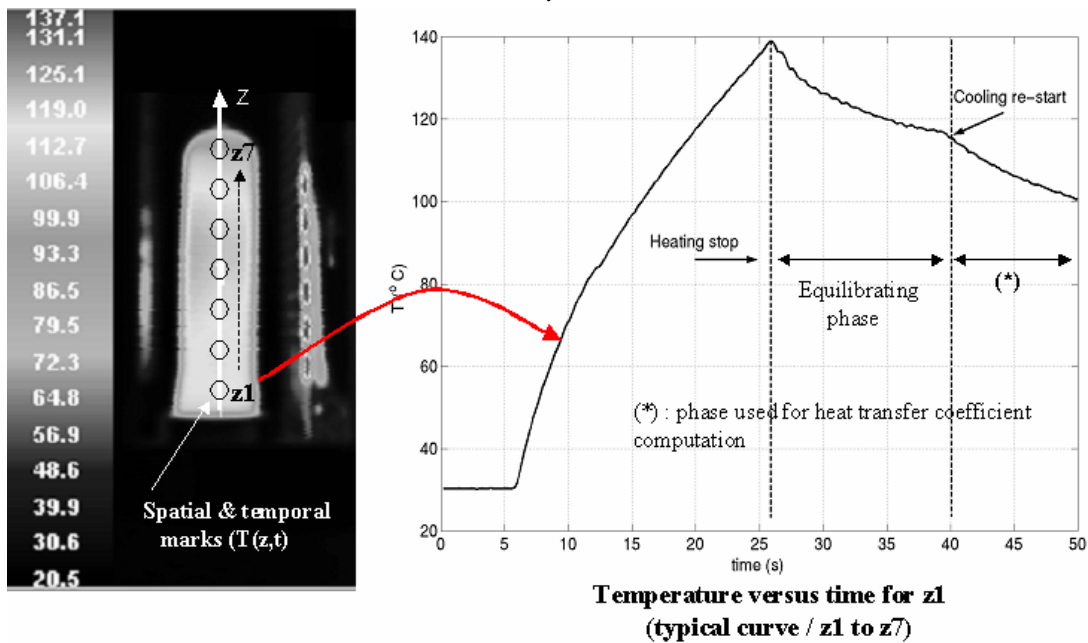


Figure 4. Areas of interest and methodology

Lock-in IR thermography for functional testing of solar cells and electronic devices

by Ottwin Breitenstein
QIRT Journal, 1, 2, pp. 151-172

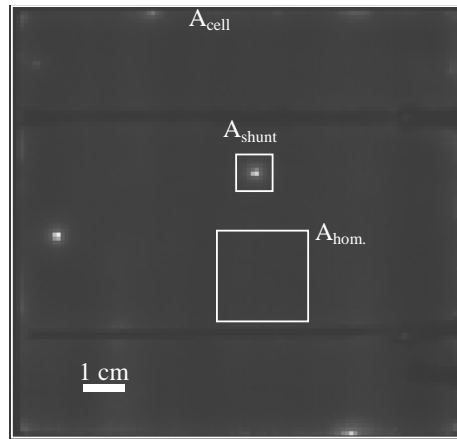


Figure 3. Lock-in thermogram (-90-image) of a solar cell with different signal averaging regions indicated

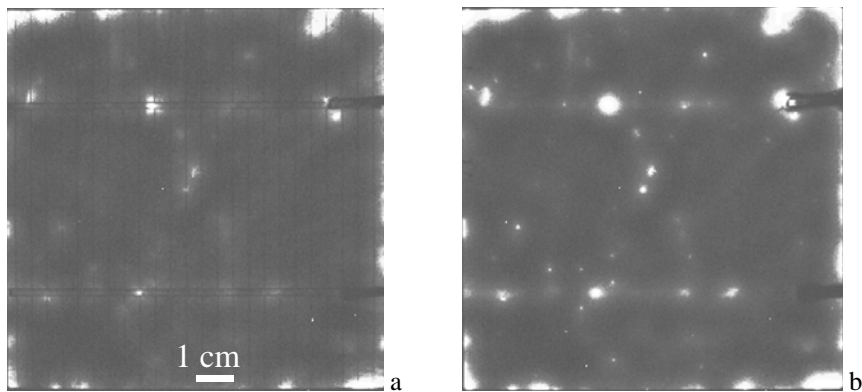


Figure 7. Amplitude images of a solar cell imaged without (a) and with (b) the application of the IR emitter foil

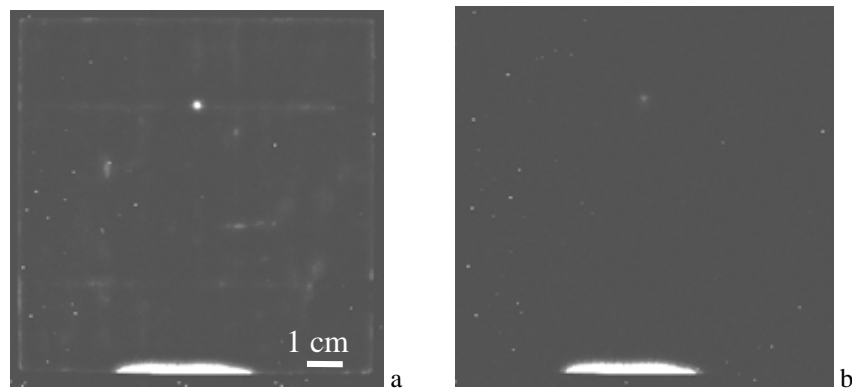


Figure 8. Amplitude images of a solar cell measured under 0.5 V forward bias (a) and under the same reverse bias (b)

QIRT Journal Iconographic Portfolio
Vol. 1 N° 2 (2004)

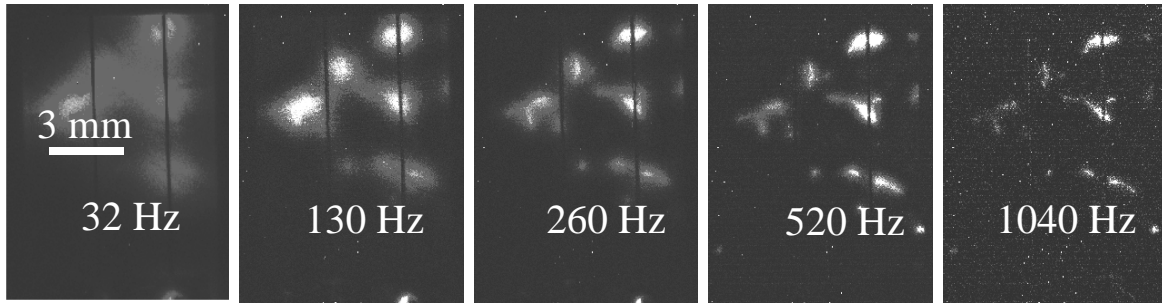


Figure 9. Amplitude images of a shunted region in a solar cell measured at different lock-in frequencies (contrast separately scaled)

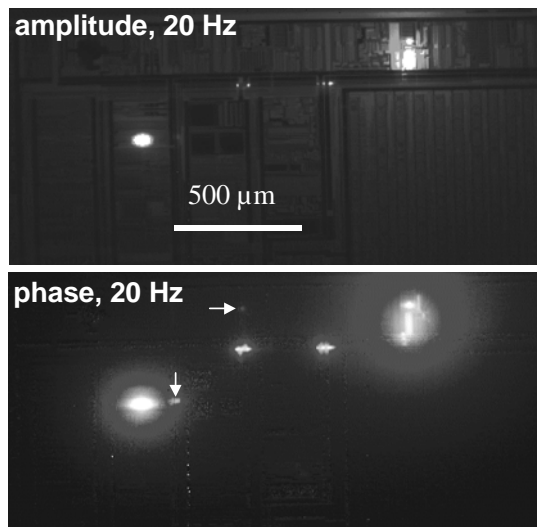


Figure 10. Amplitude and phase images of an IC containing leakage sites

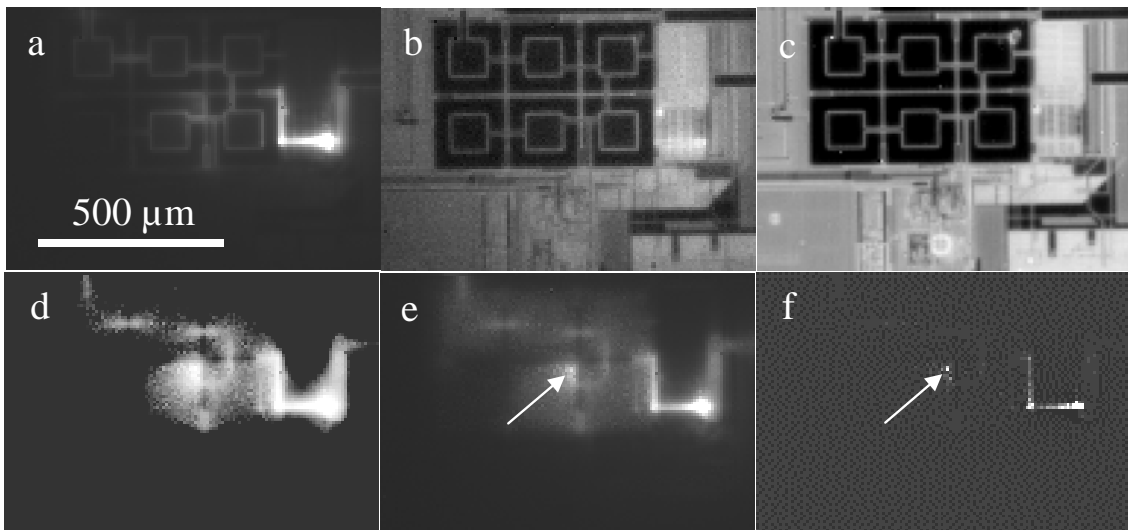


Figure 11. Different representations of lock-in thermography results of an IC containing two point heat sources. (a) 0° image, (b) -90° image, (c) topography, (d) phase image, (e) 0°/-90° image. (f) is the power distribution deconvoluted from (e).

Detecting water in aviation honeycomb structures: the quantitative approach

By Vladimir P. Vavilov and Denis A. Nesteruk

QIRT Journal, 1, 2, pp.173-184

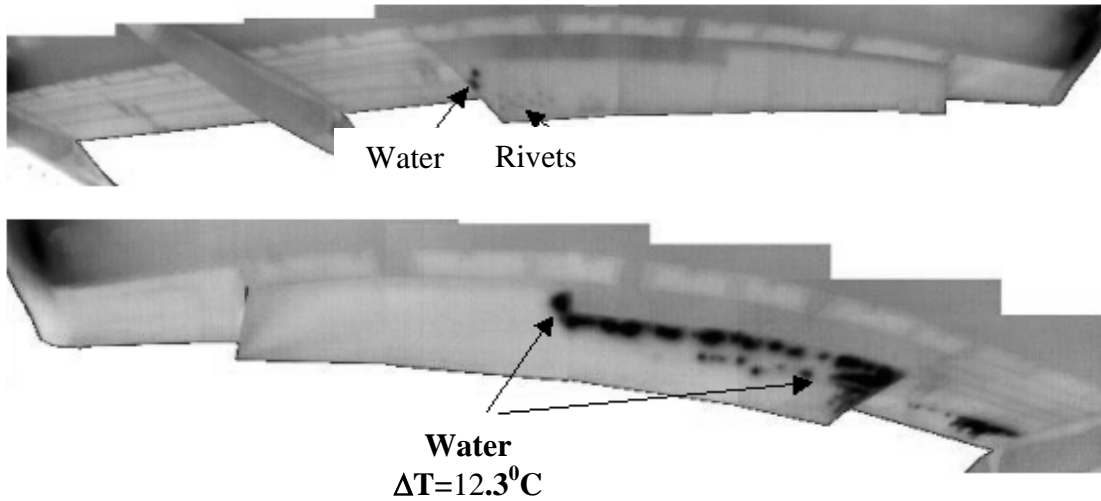


Figure 4. IR thermograms of a Toupolev-154 wings 1 hr after landing composite honeycombs)

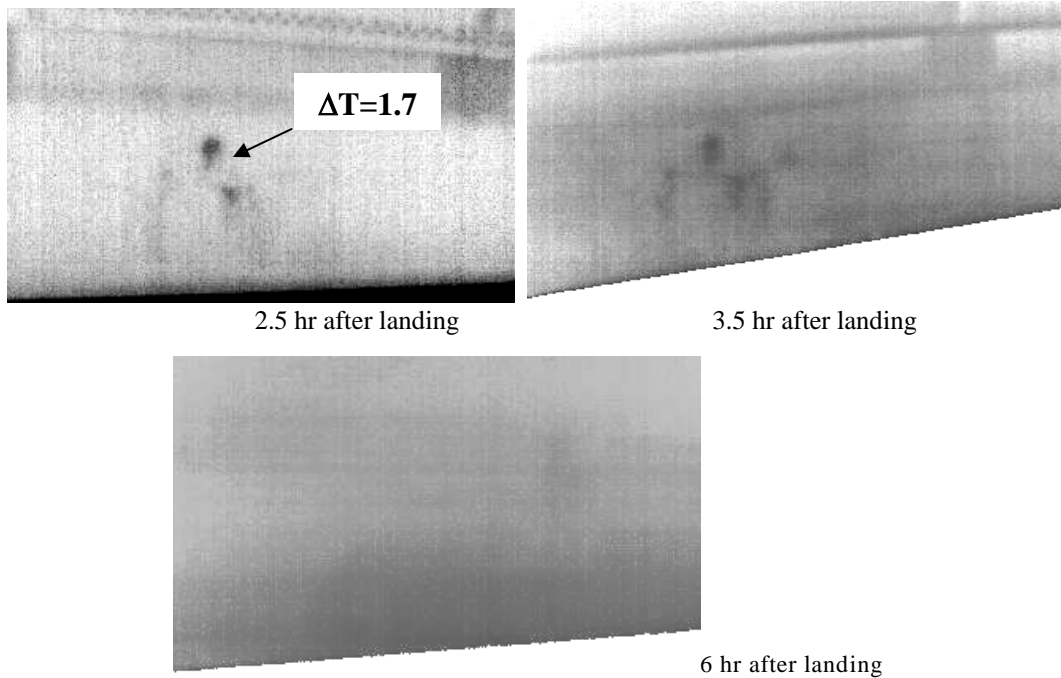


Figure 5. IR thermograms of a Toupolev-154 elevator (composite honeycombs)

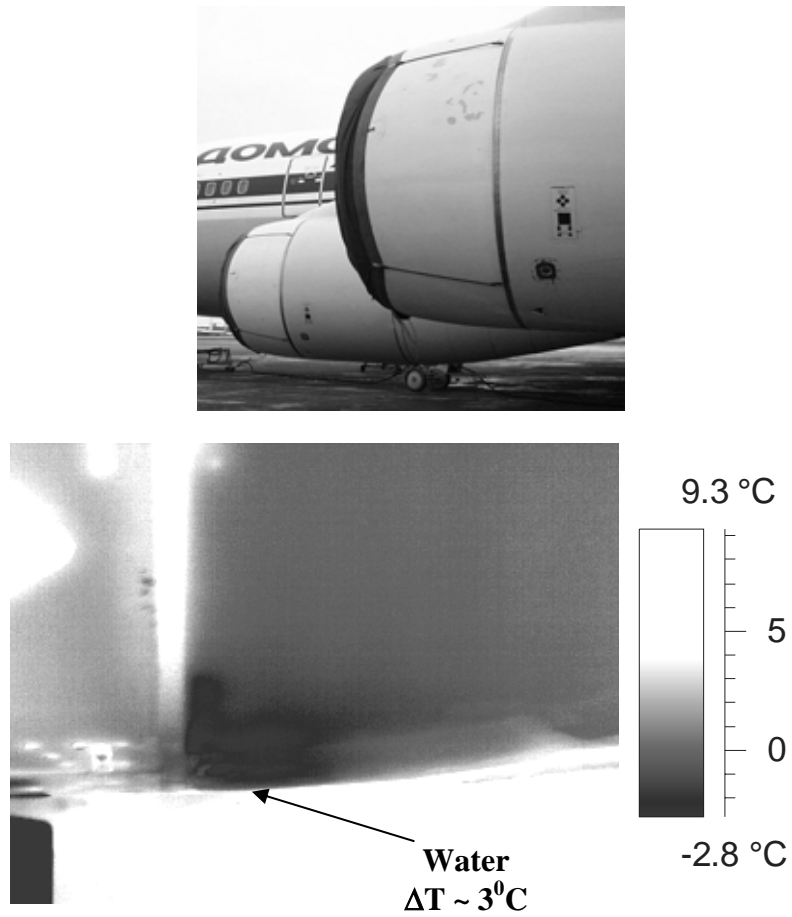


Figure 6. IR thermogram of an Ilyushin-96 engine inlet aluminum honeycombs)

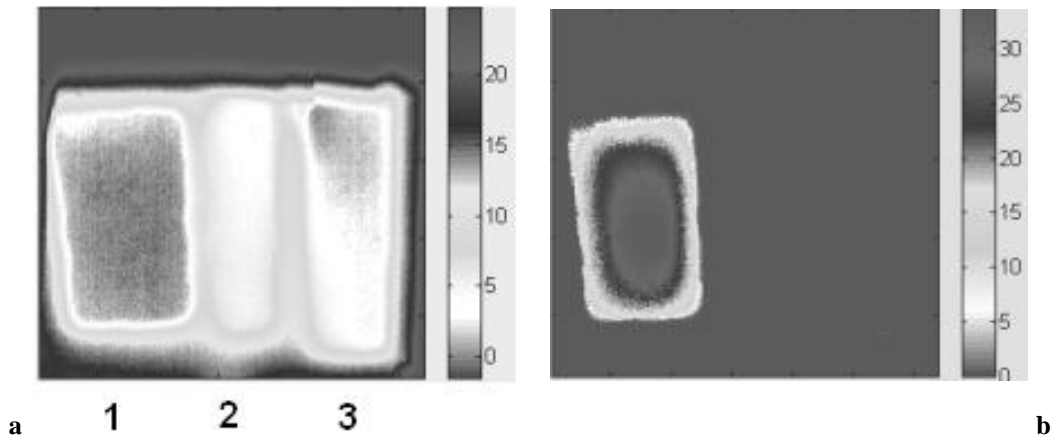


Figure 7. Enhancing water visibility by using the high water heat capacity: a) Infrared thermogram of the GFRP sample (12 min heating, 1) ice, 2) rubber, 3) steel) - b) Processing result

QIRT Journal Iconographic Portfolio
Vol. 1 N° 2 (2004)

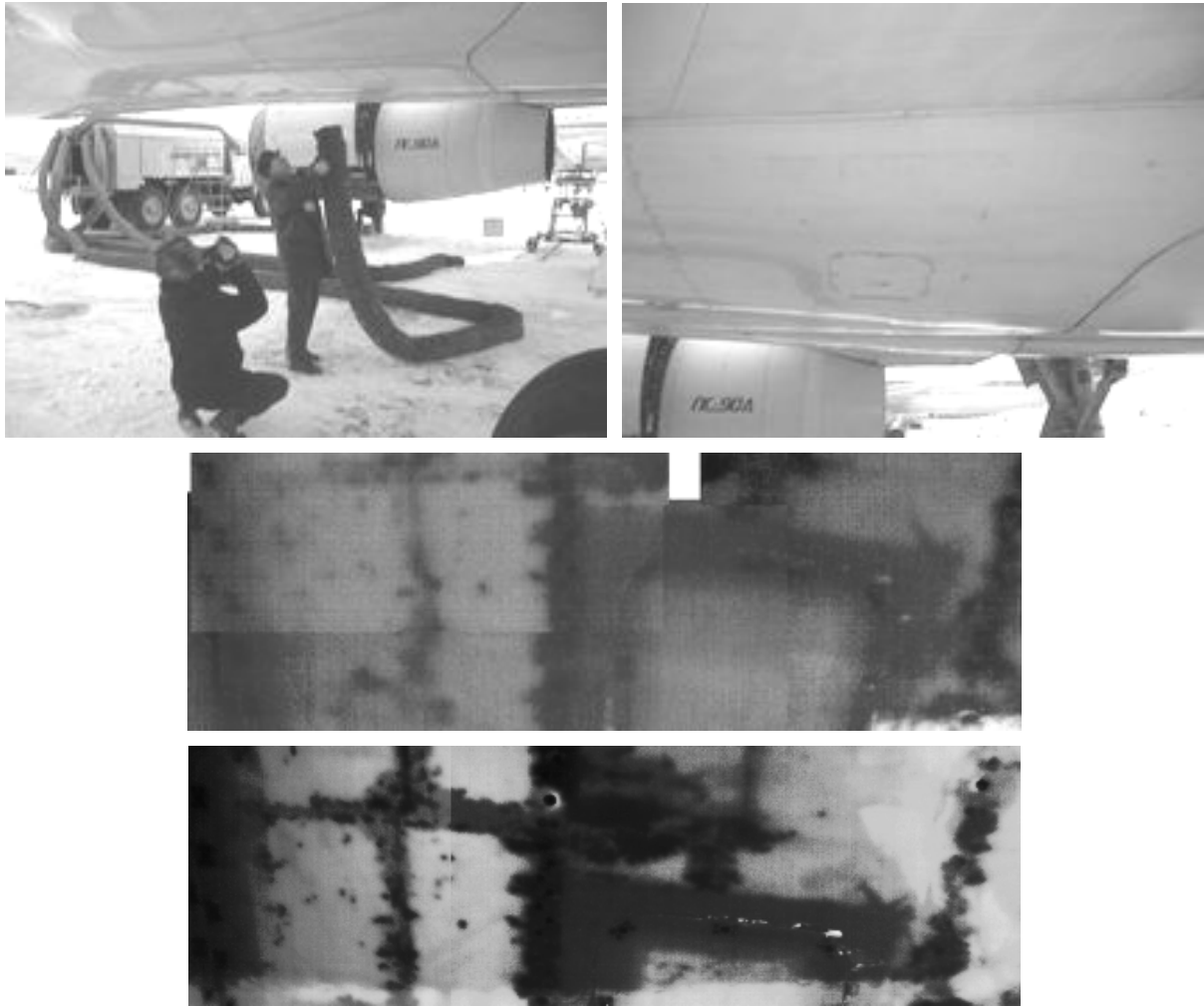


Figure 8. *Enhancing water visibility by applying additional thermal stimulation:
a) heating the fuselage of a Toupolev-154 air liner for 1 min (MP-350 air compression device), b) fuselage section photo and IR thermograms before and after heating*

QIRT Journal Iconographic Portfolio
Vol. 1 N° 2 (2004)

Monitoring acupuncture stimulation effects by infrared thermography
by Veerasak Narongpant, Stefan Datcu, Laurent Ibos, Frédéric Adnet,
Bernard Fontas, Yves Candau, David Alimi
QIRT Journal, 1, 2, pp. 185-204

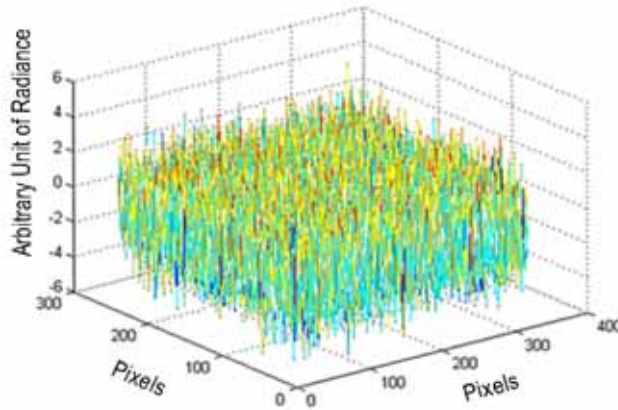


Figure 4. *The Noise of the Camera Sensors at about 303K*

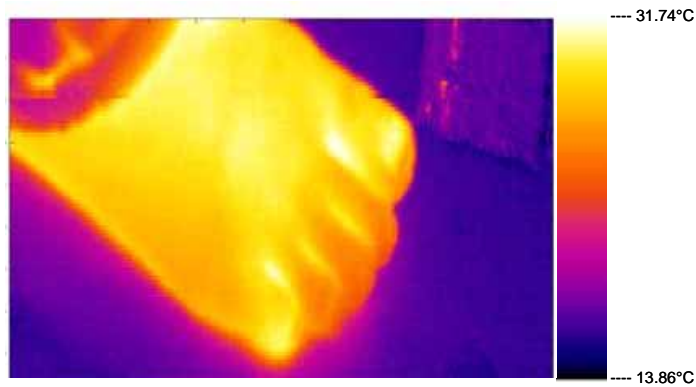


Figure 8. *Corrected thermal image, 350 seconds after the start of the test procedure*

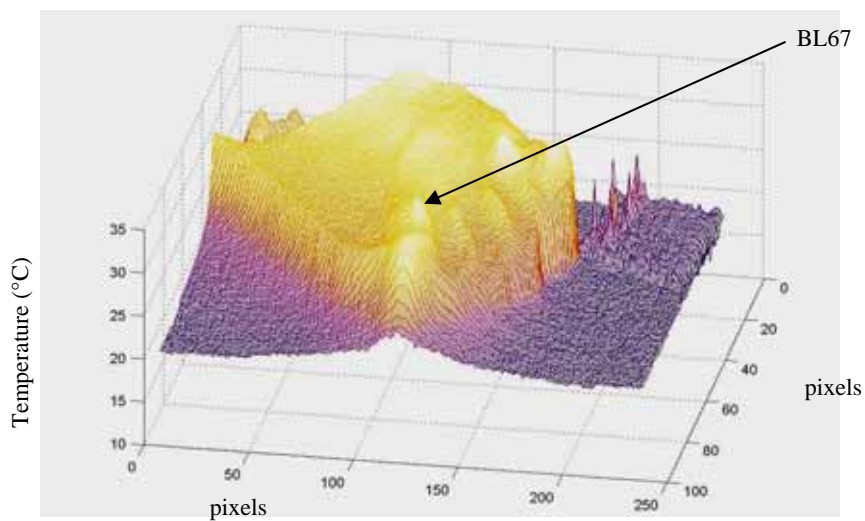


Figure 9. *3D shape of the thermal field, 350 seconds after*

QIRT Journal Iconographic Portfolio
Vol. 1 N° 2 (2004)

the experimental procedure beginning.

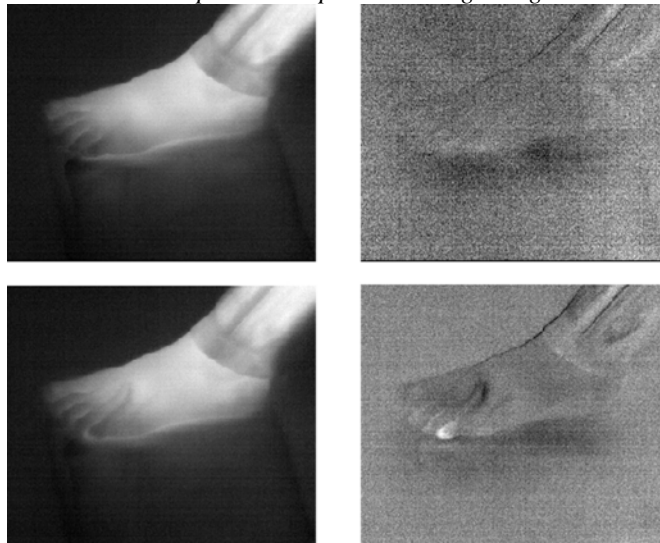


Figure 11. Above : a thermogram acquired at the first minute (before stimulation), Raw Image (left) and corresponding contrast image (right). Below : a thermogram recorded at the 4th minute (at the end of Stimulation), Raw Image (left) and corresponding to the contrast image (right) of the same volunteer.

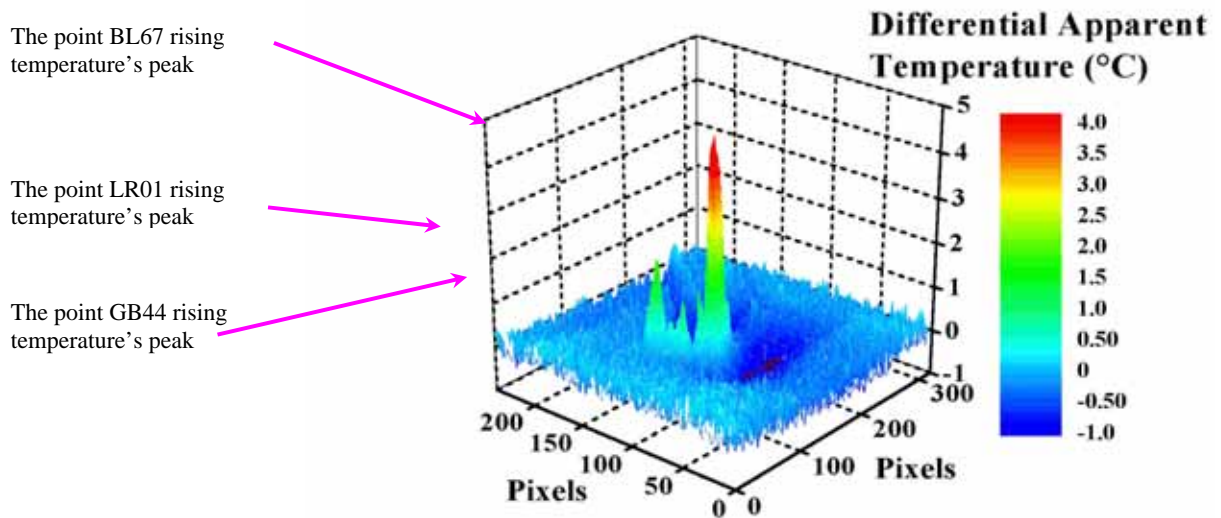


Figure 12. Apparent differential temperature on the test left foot dorsum surface of a volunteer after 2 minutes of stimulation (or at the 4th minute).

Heat flux characterisation in hot jet and flame/wall interaction by IHCP resolution coupled with infrared measurements

by Rémi Loubat, Philippe Reulet, Bruno Estebe, Pierre Millan
QIRT Journal, 1, 2, pp.205-228

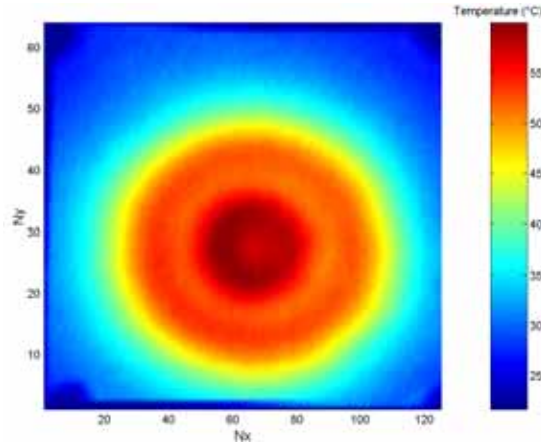


Figure 6. Measured temperature field at $t=15s$

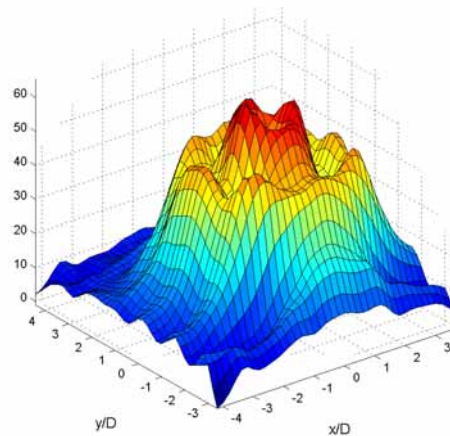


Figure 8. 3D view of recovered Nu

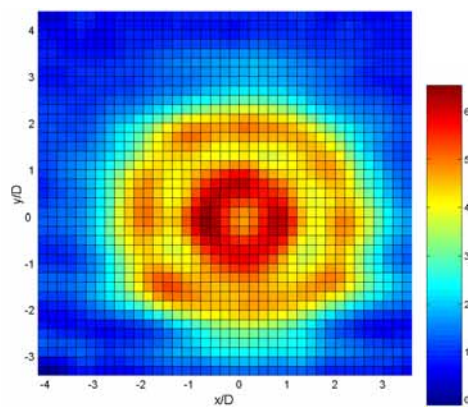


Figure 9. 2D view of recovered Nu

QIRT Journal Iconographic Portfolio
Vol. 1 N° 2 (2004)

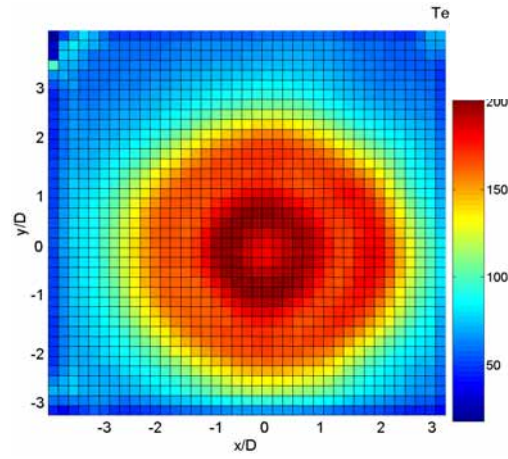


Figure 16. *Adiabatic wall temperature cartography, $H/D=2,5$, $Re=50000$*

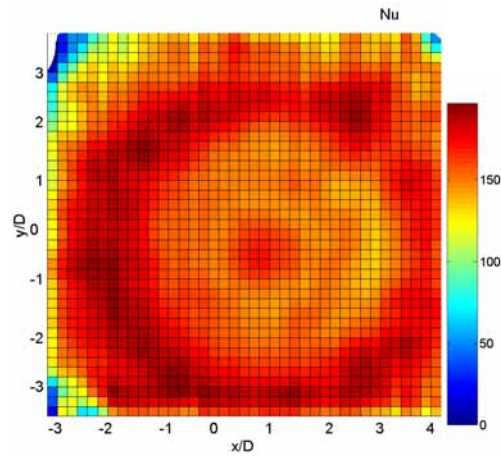


Figure 17. *Nusselt cartography, $H/D=2,5$, $Re=50000$*

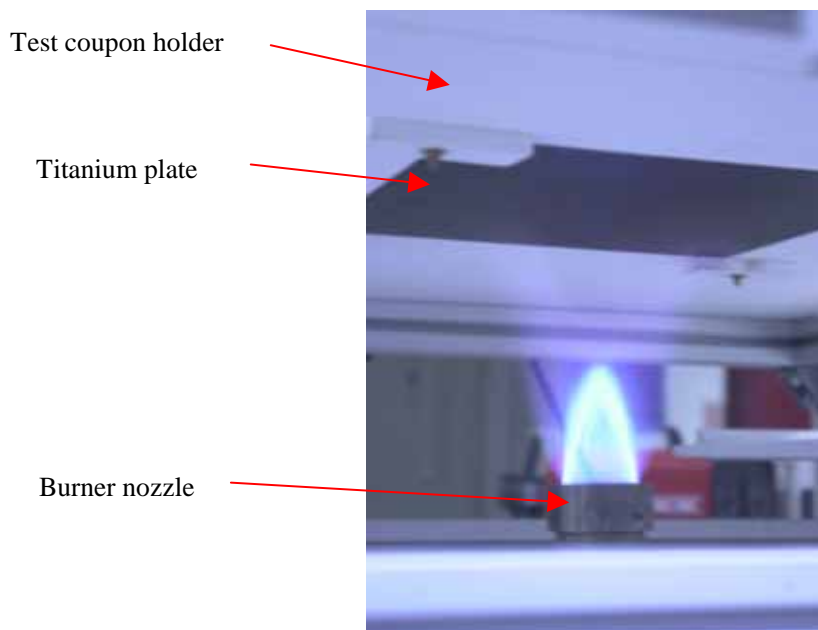


Figure 20. Flame impingement picture, $H/D=5$

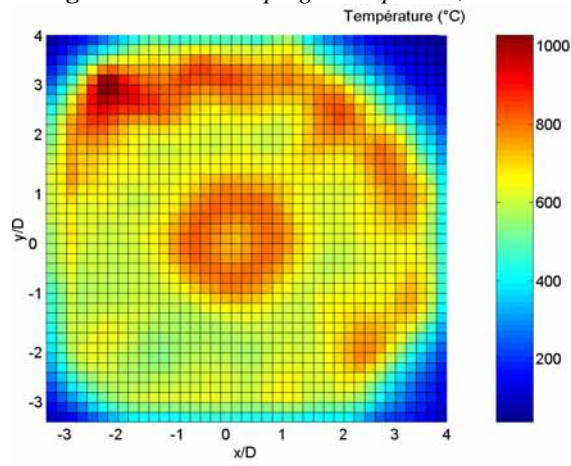


Figure 22. Adiabatic wall temperature map

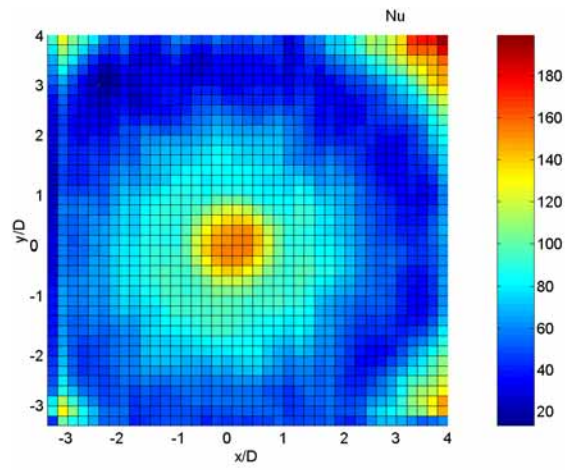


Figure 23. Associated Nusselt number

Focal plane array infrared cameras as research tools
by Hervé Pron and Christian Bissieux
QIRT Journal, 1, 2, pp.229-240

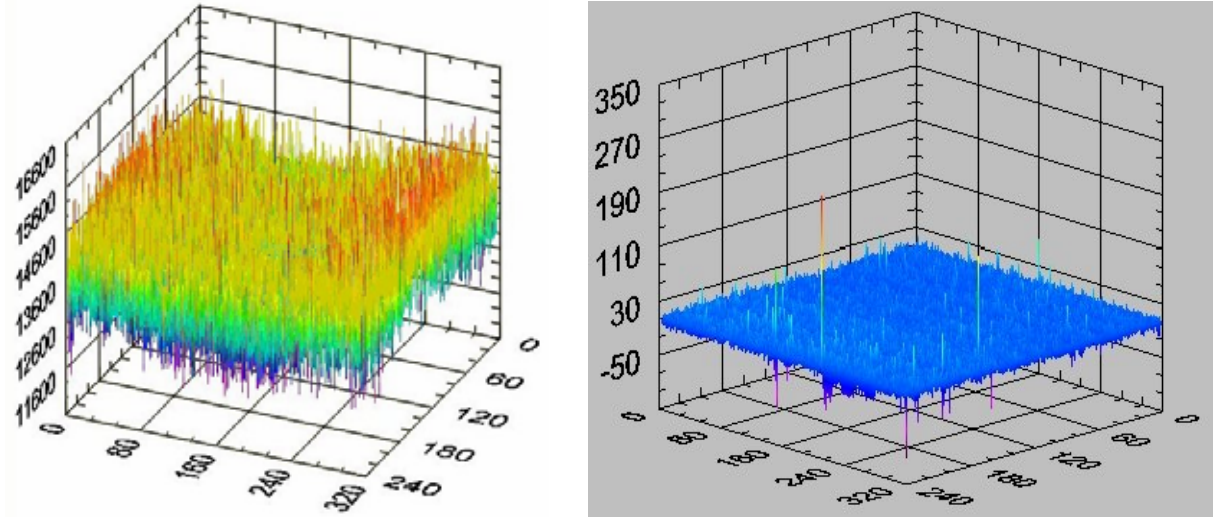


Figure 1. Left: thermal image (arbitrary units) obtained on a uniform scene, without any correction; right: noise image (arbitrary units).

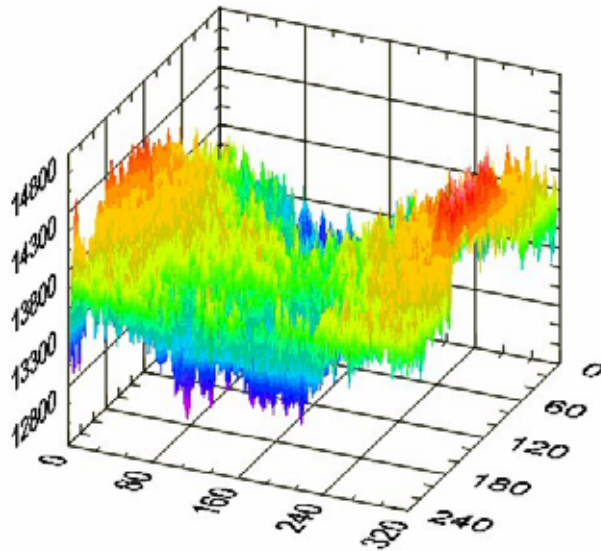


Figure 8. Same image as on left of figure 2, but after a low-pass filtering: side effects are enlightened, more especially in the wider dimension of the array (320 pixels)

QIRT Journal Iconographic Portfolio
Vol. 1 N° 2 (2004)

Local thermal diffusivity measurement
by Paolo G. Bison, Ermanno Grinzato, Sergio Marinetti
QIRT Journal, 1, 2, pp. 241-250.

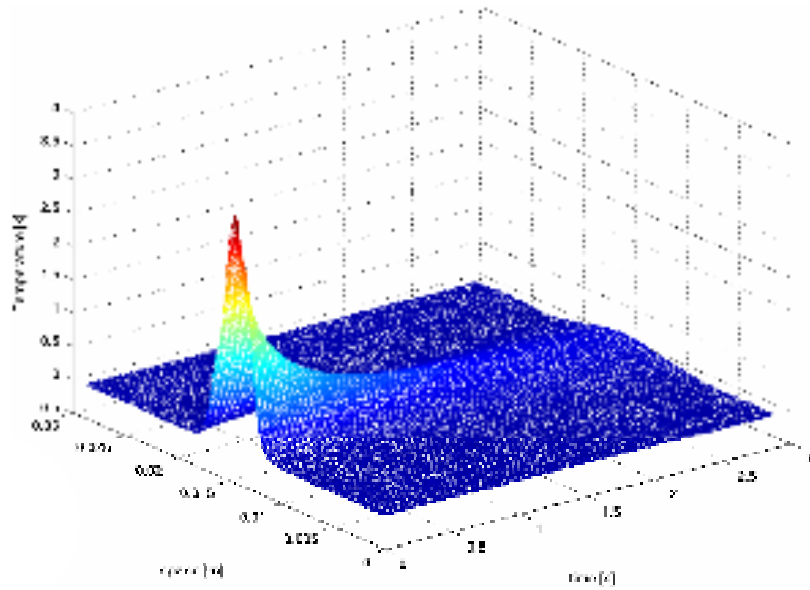


Figure 1. Averaged temperature profiles (x) vs. time (y) on a thick pietra serena block, due to a finite squared heating pulse of gaussian shape.

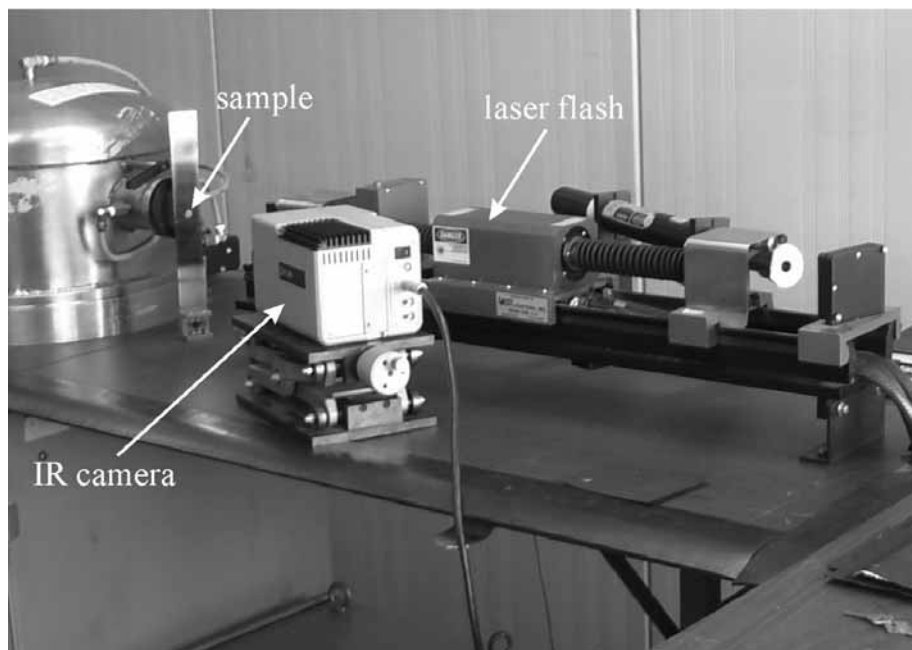


Figure 2. Experimental set up for the AISI 304 test